

Research Article

Development of a Remote Handling Robot for the Maintenance of an ITER-Like D-Shaped Vessel

Peihua Chen and Qixin Cao

State Key Laboratory of Mechanical System and Vibration, Research Institute of Robotics, Shanghai Jiao Tong University, Shanghai 200240, China

Correspondence should be addressed to Peihua Chen; cph@sjtu.edu.cn

Received 22 January 2014; Revised 20 May 2014; Accepted 20 May 2014; Published 27 August 2014

Academic Editor: Arkady Serikov

Copyright © 2014 P. Chen and Q. Cao. This is an open access article distributed under the Creative Commons Attribution License, which permits unrestricted use, distribution, and reproduction in any medium, provided the original work is properly cited.

Robotic operation is one of the major challenges in the remote maintenance of ITER vacuum vessel (VV) and future fusion reactors as inner operations of Tokamak have to be done by robots due to the internal adverse conditions. This paper introduces a novel remote handling robot (RHR) for the maintenance of ITER-like D-shaped vessel. The modular designed RHR, which is an important part of the remote handling system for ITER, consists of three parts: an omnidirectional transfer vehicle (OTV), a planar articulated arm (PAA), and an articulated teleoperated manipulator (ATM). The task of RHR is to carry processing tools, such as the viewing system, leakage detector, and electric screwdriver, to inspect and maintain the components installed inside the D-shaped vessel. The kinematics of the OTV, as well as the kinematic analyses of the PAA and ATM, is studied in this paper. Because of its special length and heavy payload, the dynamics of the PAA is also investigated through a dynamic simulation system based on robot technology middleware (RTM). The results of the path planning, workspace simulations, and dynamic simulation indicate that the RHR has good mobility together with satisfying kinematic and dynamic performances and can well accomplish its maintenance tasks in the ITER-like D-shaped vessel.

1. Introduction

The concept of magnetic confinement fusion (MCF) has long been explored to address the feasibility of nuclear fusion energy. The International Thermonuclear Experimental Reactor (ITER) project is an international collaboration to investigate the scientific and technological feasibility of MCF, which may be operated to test the future green energy roadmap as well as related facilities and technologies for the world before the middle of the 21st century [1–3]. Due to the internal adverse radiation conditions, inner operations of Tokamak have to be done by robot manipulators. Thus, robotic operation is one of the major challenges for ITER and future fusion reactors [4]. Owing to the plasma interactions, some in-vessel components are expected to erode enough to be repaired or replaced several times during the lifetime of the Tokamak. In particular, during the installation or after the shutdown, it is important and necessary for the remote handling (RH) system to execute the inspection and maintenance tasks in the vacuum vessel (VV). The RH

system is a key component in ITER operation both for scheduled maintenance and unexpected situations [5]. The maintenance of VV involves various tasks, such as transportation, inspection, dust removal, testing, and other intelligent maintenance. Whilst ensuring confinement of radioactive dust contamination inside the VV, the robot must be operated remotely because it has no radiation shielding capabilities. Design efforts have been carried on at CEA LIST to develop a long reach articulated arm for ITER-like environment, which includes the Porteur Articulé en Cellule (PAC) manipulator [6] and the articulated inspection arm (AIA) [7]. The PAC is a long reach arm with 11 degrees of freedom (DOF) and less than 30 kg weight, developed at CEA LIST mainly for AREVA-NC applications. The AIA is an 8 m long multilink carrier with five modules of 160 mm diameter dedicated to perform inspection tasks on Tore Supra, but without other maintenance functionality. Keller et al. [8] used a CEA LIST Virtual Reality simulation software to study the accessibility of the working zone located in front of the Bioshield and the feasibility of connecting/disconnecting pipes using a set

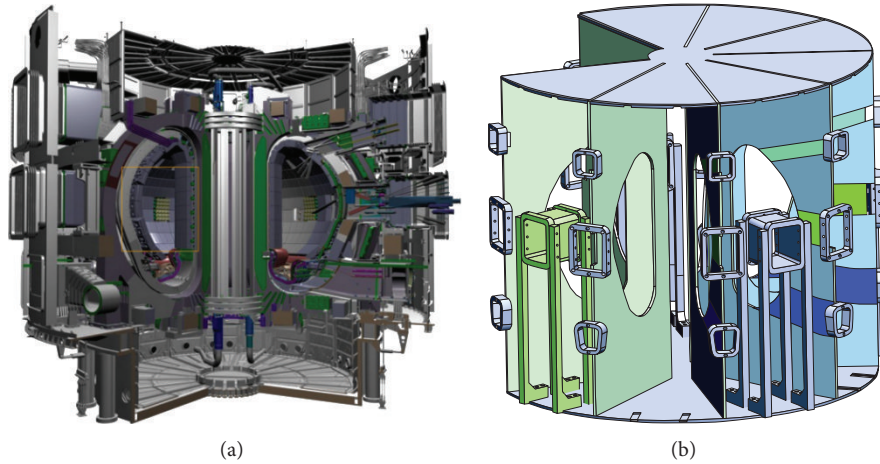


FIGURE 1: ITER Tokamak [26] and the small-scale Tokamak mockup.

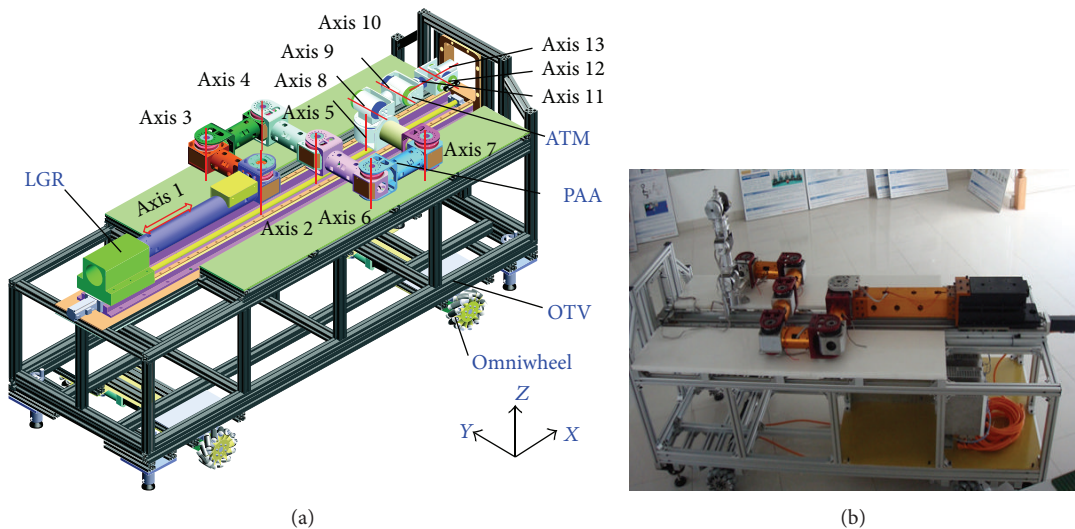


FIGURE 2: The CAD view of RHR (a) and the actual RHR (b).

of standard industrial arms. However, the industrial robot they employed was not always suitable and flexible in the ITER environment for its large size and huge controller box. As intelligent maintenance requires high accuracy and a large workspace, commercially available industrial robots cannot be directly used. To this end, a remote handling robot (RHR) was developed by the Research Institute of Robotics in Shanghai Jiao Tong University (RIR/SJTU), China, to study the intelligent maintenance and remote teleoperation of ITER-like D-shaped vessel as an MCF facility. Meanwhile, a small-scale (1/10) Tokamak mockup (Figure 1) was also designed and set up to test the robot performance and the feasibility of the remote handling system. In this project, the aim of this work is to introduce the new remote handling robot, analyze its kinematic and dynamic performances, and discuss the feasibility of the mechanical design and control method verified at least in the simulation.

The rest of this paper is organized as follows. In Section 2, the novel RHR is introduced and the important study issues

of the robot are also presented. The kinematic and dynamic analysis of the RHR is presented in Section 3. Section 4 is devoted to illustrative simulations and the corresponding results. In Section 5, conclusions are drawn and the future work is discussed.

2. The Remote Handling Robot (RHR)

The RHR, as shown in Figure 2, is a mobile robot with a multiple degrees of freedom articulated arm. The RHR is composed of an omnidirectional transfer vehicle (OTV), a planar articulated arm (PAA), and an articulated teleoperated manipulator (ATM).

The OTV has four 8'' heavy-duty Mecanum wheels and a linear guide rail (LGR) with a long travel of 2100 mm and maximum feed rate of 0.1 m/s. Although the AIA robot also has a transfer vehicle, it has a limited mobility and has to be operated by winches and guide rails on the ground [9]. In this paper, with the special mechanism of omnidirectional

wheels, the OTV is able to perform 3-DOF motion on the two-dimensional plane, which achieves translational and rotational movements simultaneously along arbitrary direction in the Tokamak room. The maximum linear velocity of the OTV is 0.3 m/s. The OTV together with LGR weighs about 226 kg and supports 200 kg loads. The LGR could make the PAA and ATM be deployed into the D-shaped vessel through the ball screw nut fitting. The Beckhoff high-performance AC servomotors are adopted as the actuators in the OTV because they are available in stainless steel designs and characterized by high dynamics, energy efficiency, low costs, and real-time (as they adopted the EtherCAT solutions). Connected to the OTV via the LGR, the PAA is a 2 m long multilink arm with a maximum payload up to 18 kg. The PAA has five modular planar joints with each module being 350 mm in length and the last link being 250 mm in length which give to the PAA six DOFs in total, as different colors indicated in Figure 2(a). Each module of the PAA mainly includes a Maxon DC servomotor, 2 bevel gears, incremental and absolute encoders, a harmonic drive gear, and EtherCAT bus driver. The bevel gears can transform the rotational direction of the motor's axis and make the output shaft of the joint vertical. The incremental and absolute encoders are used to measure the relative position of the servomotor and the absolute position of the output shaft of the joint, respectively. The harmonic drive gear is adopted here because it has no backlash, compactness and light weight, and high gear ratio, which are very important factors for a long reach multiple-link arm. The EtherCAT bus driver is employed to perform the real-time communication and control. All the elements of the module are installed inside the link and are mostly made of aluminum alloy or stainless steel. The ATM installed on the end link of the PAA is a six-DOF articulated manipulator, which weighs approximately 13 kg with a load capacity of 1.5 kg. The structure of the ATM is like an industrial robot, which also has a spherical wrist wherein the three wrist axes (axes 11–13 as shown in Figure 2(a)) intersect at a single point but is redesigned to adapt to the ITER-like D-shaped vessel environment. All the joints of the ATM are also driven by actuators with harmonic drive gears. The ATM is expected to perform the poloidal inspection and maintenance process when it is at the right toroidal position in the D-shaped vessel. With large workspace and adequate flexibility, the PAA and ATM can be deployed into the D-shaped vessel for the inspection or maintenance task through the equatorial access port. The PAA, the ATM, and the LGR make up the arm system. This paper investigates the important and necessary issues for the study of the RHR: path planning of the OTV, kinematic and dynamic analyses of the PAA, and kinematic and reachability analyses of the ATM.

As a result of the modular design of the whole robot, the operation of RHR is classified into three steps: (1) moving the OTV to the target equatorial access port and performing a docking with the port, (2) deploying the PAA and ATM into/out of the D-shaped vessel with combined motions of axes 1–7 in the horizontal plane, and (3) spreading out the ATM to execute the maintenance pertinent task. The design procedures and analysis methodologies may be adopted or

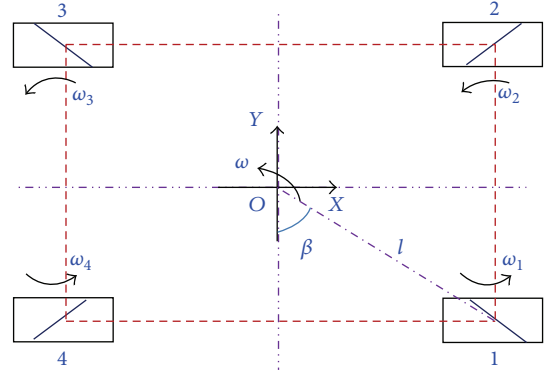


FIGURE 3: Four-wheeled OTV.

developed further by other researchers for the development of relevant remote handling robots for ITER.

3. Robot Kinematics and Dynamics

3.1. Kinematics of the OTV. To perform path planning of the OTV, the kinematics of the vehicle should first be solved. Figure 3 shows the coordinate system of the OTV and the configuration of omnidirectional wheels it adopts. The constraint equation between the angular velocity of the wheel and the velocity of the OTV $(\dot{x}_0, \dot{y}_0, \omega)^T$ is represented by

$$(\omega_1, \omega_2, \omega_3, \omega_4)^T = {}^V_W \mathbf{T} \cdot (\dot{x}_0, \dot{y}_0, \omega)^T, \quad (1)$$

where ${}^V_W \mathbf{T} \in \mathbb{R}^{4 \times 3}$ denotes the transformation matrix from the velocity of the vehicle to that of the four wheels. It is possible to obtain the equations that determine the OTV's speed related with wheels' speeds but the matrix ${}^V_W \mathbf{T}$ associated with (1) is not square. This is because the four-wheeled system is redundant. In order to obtain the omnidirectional characteristic of the OTV, the matrix ${}^V_W \mathbf{T}$ has to be full column rank; that is, $\text{rank}({}^V_W \mathbf{T}) = 3$. As for the OTV, the transformation matrix ${}^V_W \mathbf{T}$ can be derived as

$${}^V_W \mathbf{T} = \frac{1}{r} \begin{bmatrix} 1 & 1 & l(\cos \beta + \sin \beta) \\ -1 & 1 & l(\cos \beta + \sin \beta) \\ -1 & -1 & l(\cos \beta + \sin \beta) \\ 1 & -1 & l(\cos \beta + \sin \beta) \end{bmatrix}, \quad (2)$$

where r denotes the radius of the omniwheel, l denotes the distance between the center of the omniwheel and the center of the OTV, and β denotes the angle between l and the Y axis, as depicted in Figure 3.

3.2. Kinematic Analysis of the Arm System. Owing to the modular design and operation procedure of RHR as mentioned in Section 2, the kinematics of the PAA and ATM can be calculated separately in the arm system. As the LGR has only one DOF and works in the procedure of the PAA's deployment into the D-shaped vessel, it will be included in the kinematic analysis of the PAA, acting as link 1. According to D-H convention and transformation

theory between neighboring link coordinate systems, the homogeneous transformation matrix of the coordinate frame i , as represented in the coordinate frame $i-1$, can be expressed as [10]

$${}_{i-1}^i\mathbf{T} = \begin{bmatrix} c\theta_i & -s\theta_i c\alpha_i & s\theta_i s\alpha_i & a_i c\theta_i \\ s\theta_i & c\theta_i c\alpha_i & -c\theta_i s\alpha_i & a_i s\theta_i \\ 0 & s\alpha_i & c\alpha_i & d_i \\ 0 & 0 & 0 & 1 \end{bmatrix} \quad (i = 1, 2 \dots 13), \quad (3)$$

where the four quantities θ_i , a_i , d_i , and α_i are parameters associated with link i and joint i , $c \equiv \cos$, and $s \equiv \sin$. As illustrated in Section 2, once the PAA is introduced into D-shaped vessel in the toroidal direction, the axes 1-7 (Figure 2) will be fixed. The overall forward kinematics ${}_{13}^0\mathbf{T}$ for the arm system can be divided into two kinematic equations: ${}_{7}^0\mathbf{T}$ and ${}_{13}^7\mathbf{T}$; thus, we have

$$\begin{aligned} {}_{13}^0\mathbf{T} &= {}_{7}^0\mathbf{T} \cdot {}_{13}^7\mathbf{T}, \\ {}_{7}^0\mathbf{T} &= {}_1^0\mathbf{T} \cdot {}_7^1\mathbf{T} = {}_1^0\mathbf{T} \cdot {}_2^1\mathbf{T} \cdot {}_3^2\mathbf{T} \cdot {}_4^3\mathbf{T} \cdot {}_5^4\mathbf{T} \cdot {}_6^5\mathbf{T} \cdot {}_7^6\mathbf{T}, \\ {}_{13}^7\mathbf{T} &= {}_8^7\mathbf{T} \cdot {}_9^8\mathbf{T} \cdot {}_{10}^9\mathbf{T} \cdot {}_{11}^{10}\mathbf{T} \cdot {}_{12}^{11}\mathbf{T} \cdot {}_{13}^{12}\mathbf{T}. \end{aligned} \quad (4)$$

Consequently, the forward kinematics can be solved from (4) with D-H parameters. The Jacobian matrices relating the joint velocities to the linear and angular velocities of the end-effector can be obtained using the differential transformation method [10], namely, $\mathbf{J}_{AL} \in \mathbb{R}^{6 \times 7}$ for the PAA (with LGR) and $\mathbf{J}_M \in \mathbb{R}^{6 \times 6}$ for the ATM.

Inverse kinematics is required to determine the angles of the joints and displacement of the LGR, while the pose of the end-effector of the ATM is given, and is used in the position control of the arm system. Given a target pose $\mathbf{p} = (x, y, z, \alpha, \beta, \gamma)^T$, the inverse kinematics can be divided into two steps. First, the end-link pose of the PAA is derived as $\mathbf{p}_A = (x, y', 1034.5, 0, 0, \gamma)^T$, where the height of the PAA is 1034.5 mm, and y' can be obtained from the equation of the center circle of the D-shaped vessel which is $(x - 2471.96)^2 + y'^2 = 560^2$. The joint velocities of the PAA (with LGR) in joint space can be derived as

$$\dot{\mathbf{q}}_{AL} = \mathbf{J}_{AL}^+ \dot{\mathbf{p}}_A, \quad (5)$$

where $\mathbf{q}_{AL} = (q_1, q_2, q_3, q_4, q_5, q_6, q_7)^T$ is the vector of joint angles of the PAA (with LGR) and \mathbf{J}_{AL}^+ is the pseudoinverse of the Jacobian matrix \mathbf{J}_{AL} . The resolved motion rate control (RMRC) method [11], which is a kind of numerical solutions, is then chosen for the integration of the joint velocities from 0 to t_f to produce the joint angles

$$\mathbf{q}_{AL}(t_f) = \mathbf{q}_{AL,0} + \int_0^{t_f} \dot{\mathbf{q}}_{AL}(t) dt, \quad (6)$$

where $\mathbf{q}_{AL}(t_f) = \mathbf{q}_{AL}$, $\mathbf{q}_{AL,0}$ is the vector of initial joint angles of the PAA (with LGR), and $\dot{\mathbf{q}}_{AL}(t)$ is derived from (5). Second, as we could obtain ${}_{13}^0\mathbf{T}$ and ${}_{7}^0\mathbf{T}$ from \mathbf{p} and \mathbf{p}_A , respectively, ${}_{13}^7\mathbf{T}$ could be obtained from (4), and the target

pose in the ATM coordinate system could be derived as \mathbf{p}_M . Then, the joint velocities of the ATM could be derived from

$$\dot{\mathbf{q}}_M = \mathbf{J}_M^+ \dot{\mathbf{p}}_M, \quad (7)$$

where $\mathbf{q}_M = (q_8, q_9, q_{10}, q_{11}, q_{12}, q_{13})^T$ is the vector of joint angles of the ATM and \mathbf{J}_M^+ is the pseudoinverse of the Jacobian matrix \mathbf{J}_M . The joint angles of the ATM can also be obtained by utilization of the RMRC method.

3.3. Dynamics of the PAA. Aside from the kinematics of the arm system, dynamics is another important aspect for a robot, especially for the PAA in this RHR because of the special length and heavy payload of the arm. The dynamics also has a significant impact on the development of the mechanical design and control system. Excellent dynamic performance contributes to a simple and light structure, as well as a simple and reliable control system. Following [12], in the absence of friction and disturbance, the dynamics of the PAA can be described as

$$\mathbf{M}(\mathbf{q}) \ddot{\mathbf{q}} + \mathbf{C}(\mathbf{q}, \dot{\mathbf{q}}) \dot{\mathbf{q}} + \mathbf{g}(\mathbf{q}) = \boldsymbol{\tau}, \quad (8)$$

where $\mathbf{q} \in \mathbb{R}^6$ is the vector of the generalized joint coordinates, $\boldsymbol{\tau} \in \mathbb{R}^6$ is the vector of the generalized torques acting on the PAA, $\mathbf{M}(\mathbf{q}) \in \mathbb{R}^{6 \times 6}$ is the inertia matrix, $\mathbf{C}(\mathbf{q}, \dot{\mathbf{q}}) \dot{\mathbf{q}} \in \mathbb{R}^6$ is the vector of Coriolis/centrifugal forces, and $\mathbf{g}(\mathbf{q}) = \partial \mathbf{H}(\mathbf{q}) / \partial \mathbf{q} \in \mathbb{R}^6$ is the gradient of the potential function $\mathbf{H}(\mathbf{q})$.

However, the computational cost of (8) is enormous [10], $O(n^4)$, which made it infeasible for real-time use in actual application. So, the recursive Newton-Euler algorithm (RNEA) with $O(n)$ computational complexity [13] is used to compute the inverse dynamics of the PAA. The RNEA starts at the base and works outward adding the velocity and acceleration of each joint in order to determine the velocity and acceleration of each link. Then, working from the end-link back to the base, it computes the forces and moments acting on each link and thus the joint torques. The RNEA can be written in the form

$$\boldsymbol{\tau} = \mathbf{ID}(\mathbf{q}, \dot{\mathbf{q}}, \ddot{\mathbf{q}}). \quad (9)$$

During the motion control of the PAA, there will be uncertainty in the inertia parameters, unmodeled forces, or external disturbances. Thus, a feedback term is needed to compensate for any errors due to the uncertainty of the robot dynamics. Here, the inverse dynamics control method [14, 15] is used to compute the joint torques and deal with the dynamic uncertainty, wherein a PD controller is adopted as the feedback term. The inverse dynamics control method can be given by

$$\boldsymbol{\tau} = \mathbf{ID}(\mathbf{q}, \dot{\mathbf{q}}, \ddot{\mathbf{q}}_d + \mathbf{K}_D \dot{\mathbf{e}} + \mathbf{K}_P \mathbf{e}), \quad (10)$$

where $\mathbf{e} = \mathbf{q}_d - \mathbf{q}$ is the vector of joint position errors, \mathbf{K}_P and \mathbf{K}_D are the position and velocity gain matrices, respectively, and $\ddot{\mathbf{q}} = \ddot{\mathbf{q}}_d + \mathbf{K}_D \dot{\mathbf{e}} + \mathbf{K}_P \mathbf{e}$. The control law of (10), which contains the terms $\mathbf{K}_P \mathbf{e} + \mathbf{K}_D \dot{\mathbf{e}}$ that are actually premultiplied by the inertial matrix, is not a linear controller as the PD

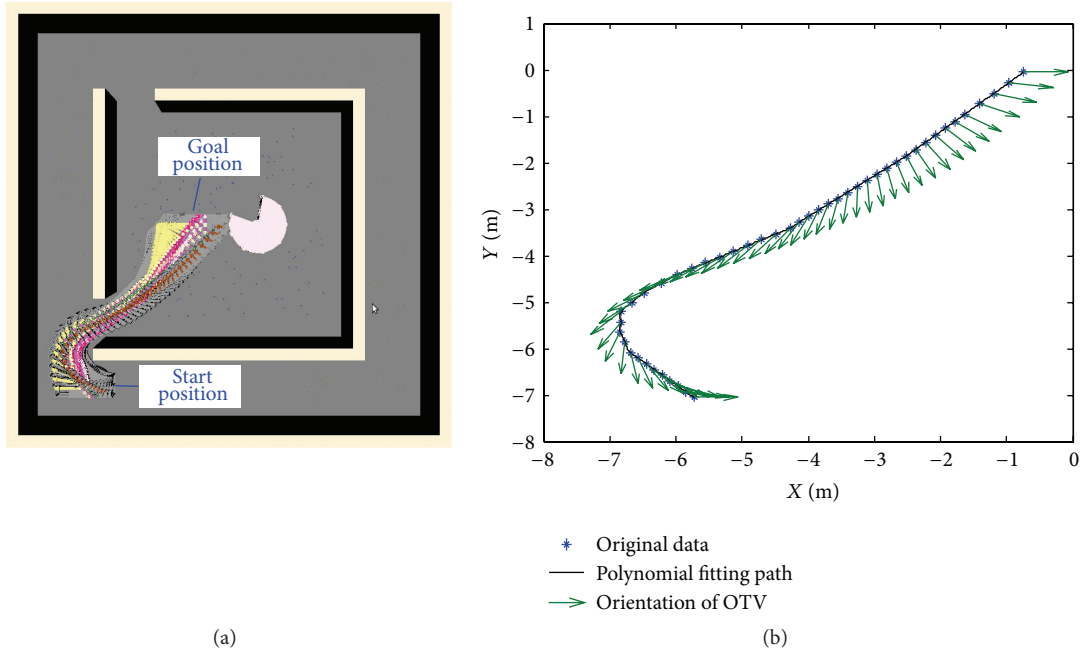


FIGURE 4: Planning result of RRT-Connect planner (a) and the polynomial fitting path with respect to the orientation of the vehicle (b).

controller. The inverse dynamics control is one of the model-based motion control approaches for manipulators. In our previous work [15], we have discussed the details about the inverse dynamics control, its application on the trajectory control of the articulated robot, and comparisons with PD controller. In practice, the joint space trajectory is always planned first; that is, the desired trajectory of motion $\mathbf{q}_d(t)$ and its derivatives $\dot{\mathbf{q}}_d(t)$ and $\ddot{\mathbf{q}}_d(t)$ could be obtained. Thus, we usually use $ID(\mathbf{q}_d, \dot{\mathbf{q}}_d, \ddot{\mathbf{q}}_d + \mathbf{K}_D\dot{\mathbf{e}} + \mathbf{K}_P\mathbf{e})$ to compute the required joint torques to achieve the desired motions of the robot [16]. The linear error equation is then derived as

$$\ddot{\mathbf{e}} + \mathbf{K}_D\dot{\mathbf{e}} + \mathbf{K}_P\mathbf{e} = 0. \quad (11)$$

If the gain matrices \mathbf{K}_P and \mathbf{K}_D are chosen as symmetric positive-definite matrices, then the closed-loop system is linear, decoupled, and globally stable.

4. Experimental Results

4.1. Path Planning of the OTV. Since the environment of Tokamak building is comprised of static and well-structured scenarios, the path planning of the OTV could be executed offline, and the planned paths may be stored in a teaching file for further use. Fonte et al. [17] proposed a motion planning methodology for the transfer cask system (TCS) to operate in the cluttered and static ITER environment. Recently, they proposed the cask and plug remote handling system (CPRHS) to provide the means for the remote transfer of invessel components and remote handling equipment between the hot cell building (HCB) and the Tokamak building in ITER along predefined optimized trajectories [18–20]. However,

they used a rhombic kinematic configuration with two pairs of drivable and steerable wheels in the vehicle which has a limited mobility comparing to the OTV adopted in this paper. In addition, challenges about how to evaluate the cell decompositions and how to improve the efficiency of the path planning still exist. In this paper, we employed the open motion planning library (OMPL) [21] and the RRT-Connect [22] algorithm to perform the path planning between a start position and the target position for docking to the equatorial access port, as presented in Figure 4(a). The path planning methodology takes the geometry of the OTV into consideration, which will shorten the planning time. The average runtime of the path planning is approximately 0.26 s on a machine with an Intel i5-2400 CPU (3.1 Ghz) and 4 GB RAM (the same hereinafter). However, the initial path does not guarantee the path smoothness. Thus, the polynomial fitting method is utilized to fit the discrete trajectory data and obtain a smooth and continuous path for the robot. The polynomial fitting path is shown in Figure 4(b), wherein the green arrows denote the OTV orientation. After the OTV moves to the target position which is always a little distance away from the equatorial access port, it will execute the docking process as introduced in Section 2. During this process, the control room will teleoperate the OTV remotely via EtherCAT bus to move towards the equatorial access port, wherein the orientation of the OTV could also be adjusted remotely and conveniently. In order to realize the docking to the equatorial access port of the ITER-like D-shaped vessel, we designed a pair of mounting flanges on the OTV and the access port, respectively. In the mounting flange on the OTV side, there are two taper holes for guiding and aligning to the circular truncated cone fixed on the equatorial access port.

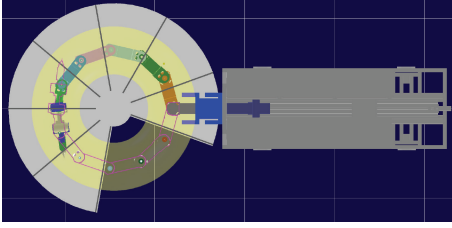


FIGURE 5: Schematic view of RHR integration on the Tokamak mockup (top view).

4.2. Workspace Simulation of the PAA. A large workspace serves an important function for the PAA during the maintenance work in the D-shaped vessel. Concretely, the PAA could reach as much area as possible in the horizontal plane of the D-shaped vessel from the same access port; efficiency will be improved and the number of robots needed to fulfill the maintenance of ITER-like D-shaped vessel will be reduced. Peng et al. [23] introduced a long reach multiarticulated manipulator with ten degrees of freedom (DOFs) formed by a main robot and an end-effector. However, this robot could not cover all of the horizontal space in the EAST VV from the same access port. In this paper, the PAA of RHR could reach almost every corner of the horizontal plane of the D-shaped vessel with the associated movements of the LGR and PAA, as depicted in Figure 5.

The workspace of the PAA has been investigated by MATLAB simulation utilizing Monte Carlo method as a random sampling numerical approach to create thousands of random joint series in the joint space. The forward kinematic model is then used to transform the joint space to the Cartesian space of the PAA's end-effector, which determines the workspace of the PAA. Figure 6 shows the workspace of the PAA (displacement of the LGR is 1500 mm) within the D-shaped vessel in the horizontal plane. Different colors denote different density of the reachable workspace at that position, wherein the amount of possible reachable configuration becomes larger when the color changes from green to red.

According to the definition of kinematic redundancy of a robot in literature [24], the PAA together with the LGR is kinematically redundant as the dimension of the joint space is greater than the dimension of end-effector space. During the whole manipulator's insertion into the D-shaped vessel, the PAA has to be deployed into the equatorial access port first via motion planning. In this process, given a target posture, inverse kinematics of the PAA (with LGR) is employed to transform from task space to joint space. When the goal configuration in the joint space is obtained and valid, the motion planning based on RRT-Connect [22] is adopted to find a collision-free path from the start configuration to the goal configuration.

4.3. Workspace Simulation of the ATM. The ATM is expected to perform the maintenance work inside the D-shaped vessel after being brought to a right toroidal position by the PAA. Owing to the planar feature of the PAA, the ATM needs to reach as much space as possible with its own mechanical

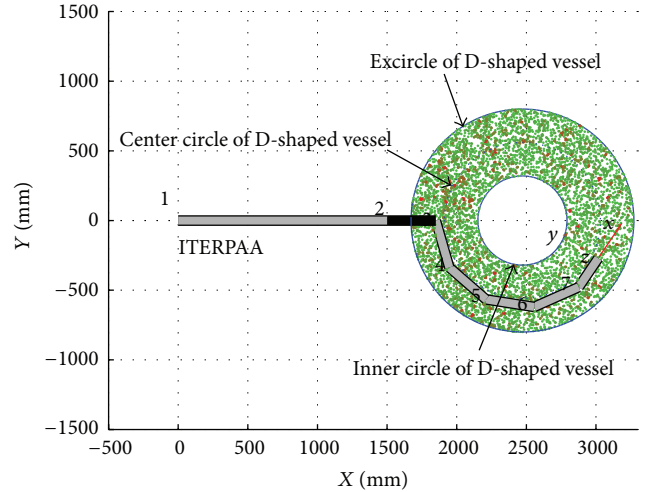


FIGURE 6: Workspace of the PAA in the horizontal plane inside the D-shaped vessel.

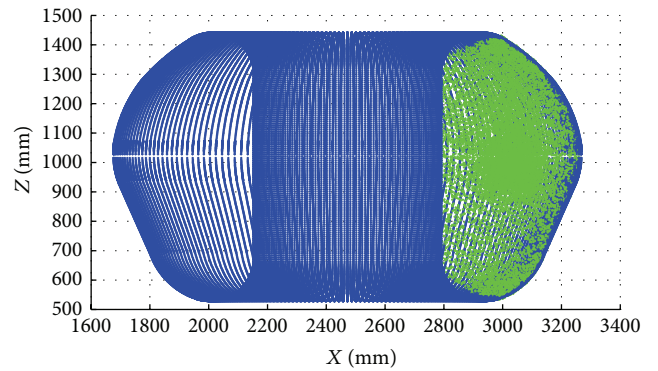


FIGURE 7: Workspace simulation of the ATM in the D-shaped vessel.

structure so that the maintenance work can be done. Considering the workspace requirement and the size of a D-shaped cross section of the vessel, we designed a six-DOF ATM with optimized link lengths and mass distribution (see Figure 2). As the PAA can reach almost every corner in the horizontal plane of the D-shaped vessel, only the reachability of the ATM at one position along the toroidal direction has to be analyzed, for example, the position on the center circle of D-shaped vessel. Figure 7 depicts that the PAA deploys the ATM to the position of (2931.96, 0, 959.5), where the pedestal height of the ATM is 75 mm lower than that of the PAA. The workspace of the ATM (green color in the figure) is simulated with respect to the cross section of the 3D D-shaped vessel model (blue color in the figure) in MATLAB. The result shows a perfect coverage of the inner surface of the vessel in the D-shaped cross section.

4.4. Dynamic Simulation of the PAA. To investigate the dynamic properties of the PAA, a dynamic simulation system based on robot technology middleware (RTM) [25] was developed to study the dynamic performance for the purpose of verifying the current design's reliability and investigating

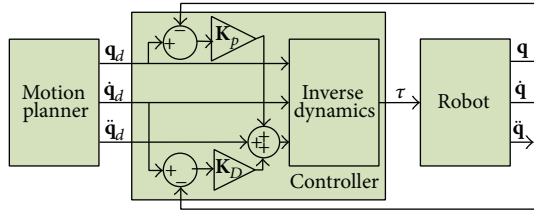


FIGURE 8: Dynamic simulation system block scheme.

the control algorithm’s feasibility, as depicted in Figure 8. In the dynamic simulation, we used the inverse dynamics control method which is based on the RNEA to calculate the joint torques that have to be applied on the PAA’s joints. The implementation of (10) is realized in the controller module of the dynamic simulation system, as shown in Figure 8. In order to make use of the planned data created by the motion planner to obtain the computed torques for controlling the motion of the robot, we make the inputs of the inverse dynamics controller as \mathbf{q}_d , $\dot{\mathbf{q}}_d$, and $\ddot{\mathbf{q}}_d + \mathbf{K}_D \dot{\mathbf{e}} + \mathbf{K}_P \mathbf{e}$ to compute the required joint torques. The PAA is required to follow the path from the initial position (Figure 2) to the fully unfolded position (Figure 5) with or without 15 kg payload (include the mass of the ATM). The LGR is fixed during the simulation. The controller gains are chosen as $\mathbf{K}_P = 10000\mathbf{I}$ and $\mathbf{K}_D = 120\mathbf{I}$. The motion planning for the path is done with joint space planning and Cartesian space planning in the motion planner module. From the simulation, the joint coordinates, velocities, accelerations, and torques along the path can be obtained. The desired joint trajectories are chosen to be fifth-order polynomials and are shown in Figure 9. The joint velocity evolution of the PAA is presented in Figure 10. The results reveal that the motions, velocities, and accelerations of each joint evolved smoothly. Figure 11 shows a comparison of torque evolution under no payload with that under a payload of 15 kg. The torque value of each joint is in the limitation of corresponding selected actuator. The value is larger when the PAA has a payload.

5. Conclusions and Future Work

In this paper, the kinematic and dynamic analyses of a novel RHR have been studied for the remote maintenance of an ITER-like D-shaped vessel. The RHR consists of three parts, namely, the OTV, the PAA, and the ATM. The PAA is connected to the OTV through the LGR, whereas the ATM is installed on the end link of the PAA. The path planning and trajectory optimization of the OTV show that the RHR has good mobility in the vehicle part. The modular design of the robot facilitates simple development and easy integration and offers the RHR simple kinematic formulations. The kinematic analysis of the arm system and the workspace simulations of the PAA and ATM show that the RHR is sufficiently dexterous to reach the needed workspace through the combined motions of the PAA and ATM such that at least one RHR is required to fulfill the inspection or maintenance tasks of the whole invessel surfaces. Workspace simulations of the PAA and ATM, together with the dynamic simulation of

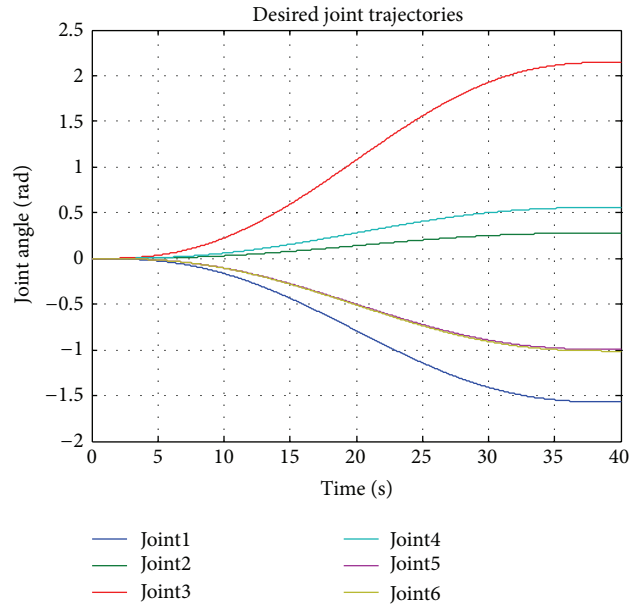


FIGURE 9: Desired joint trajectories for the dynamic simulation.

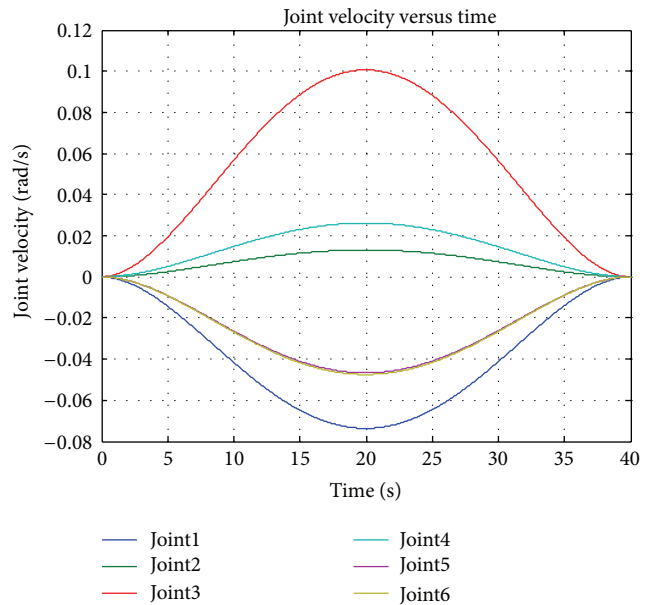


FIGURE 10: Joint velocity evolution during the dynamic simulation.

the PAA using the inverse dynamics control, were studied and integrated into the design process to verify the mechanical design and feasibility of control algorithms. All simulations indicated that the RHR has superior kinematic and dynamic performances and proved the feasibility and reliability of the robot in terms of the maintenance of the ITER-like D-shaped vessel.

Considerable design, analysis, and investigations are required to move from the present status (mechanical design, supported by simulation analysis) to the final design and application on the actual remote handling system. Robustness, reliability, and flexibility of the RHR will be tested and

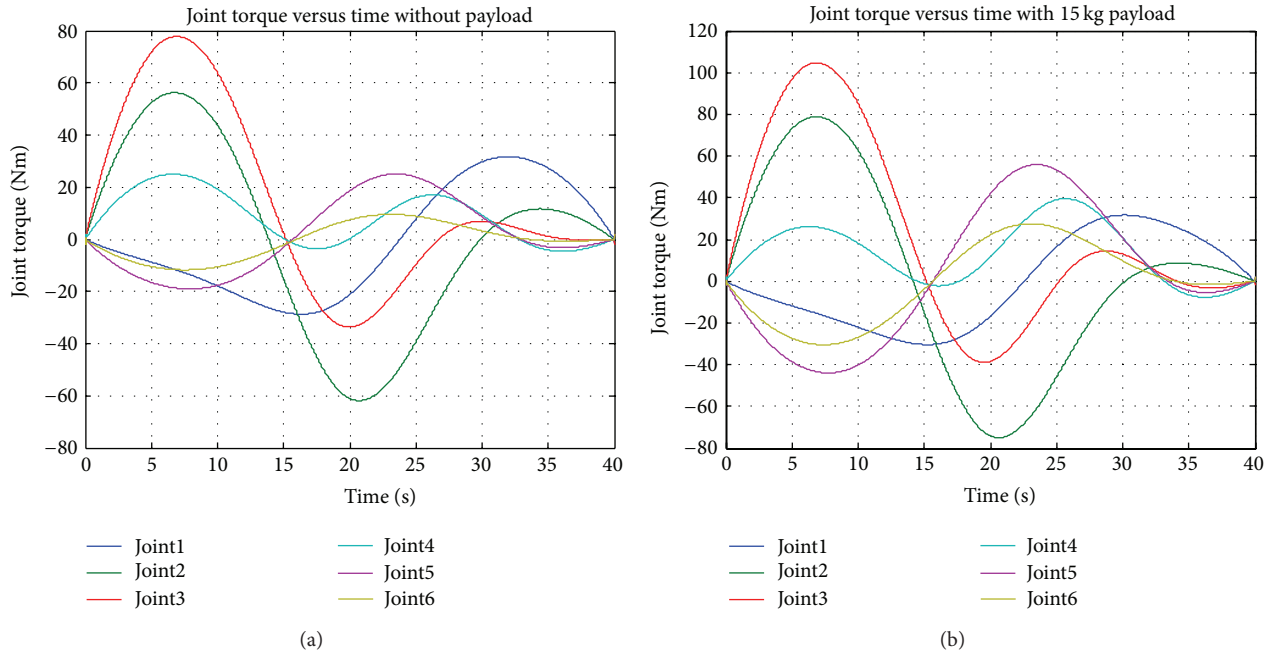


FIGURE 11: Comparison of torque evolution under no payload (a) and with 15 kg payload (b).

improved during successive operating campaigns in a routine maintenance mode in the future.

Conflict of Interests

The authors declare that there is no conflict of interests regarding the publication of this paper.

Acknowledgments

This work is supported by the Major State Basic Research Development Program of China under Grant no. 2011GB113005 and in part by the National High Technology Research and Development Program of China under Grant no. 2012AA041403. The authors would also like to thank the anonymous reviewers and the editor for their helpful comments on the paper.

References

- [1] D. Clery, "ITER's \$12 billion gamble," *Science*, vol. 314, no. 5797, pp. 238–242, 2006.
- [2] A. E. Costley, "Towards diagnostics for a fusion reactor," *IEEE Transactions on Plasma Science*, vol. 38, no. 10, pp. 2934–2943, 2010.
- [3] G. Federici, R. Kemp, D. Ward et al., "Overview of EU DEMO design and RD activities," *Fusion Engineering and Design*, 2014.
- [4] L. Gargiulo, P. Bayetti, V. Bruno et al., "Operation of an ITER relevant inspection robot on Tore Supra tokamak," *Fusion Engineering and Design*, vol. 84, no. 2–6, pp. 220–223, 2009.
- [5] I. Ribeiro, C. Damiani, A. Tesini, S. Kakudate, M. Siuko, and C. Neri, "The remote handling systems for ITER," *Fusion Engineering and Design*, vol. 86, no. 6–8, pp. 471–477, 2011.
- [6] J. Chaifoun, C. Bidard, D. Keller, Y. Perrot, and G. Piolain, "Design and flexible modeling of a long reach articulated carrier for inspection," in *Proceedings of the IEEE/RSJ International Conference on Intelligent Robots and Systems (IROS '07)*, pp. 4013–4019, November 2007.
- [7] L. Gargiulo, P. Bayetti, V. Bruno et al., "Development of an ITER relevant inspection robot," *Fusion Engineering and Design*, vol. 83, no. 10–12, pp. 1833–1836, 2008.
- [8] D. Keller, C. Dechelle, L. Doceul et al., "ITER Equatorial Port plug engineering: design and remote handling activities supported by Virtual Reality tools," *Fusion Engineering and Design*, vol. 86, no. 9–11, pp. 2105–2108, 2011.
- [9] D. Keller, J.-P. Friconneau, and Y. Perrot, "An ITER relevant robot for remote handling: on the road to operation on Tore Supra," in *Advances in Service Robotics*, H. S. Ahn, Ed., InTech, Rijeka, Croatia, 2008.
- [10] M. W. Spong, S. Hutchinson, and M. Vidyasagar, *Robot Modeling and Control*, John Wiley & Sons, New York, NY, USA, 2006.
- [11] D. E. Whitney, "Resolved motion rate control of manipulators and human prostheses," *IEEE Transactions on Man-Machine Systems*, vol. 10, no. 2, pp. 47–53, 1969.
- [12] J. J. Craig, *Introduction to Robotics: Mechanics and Control*, Pearson Education, New York, NY, USA, 3rd edition, 2005.
- [13] R. Featherstone, *Rigid Body Dynamics Algorithms*, Springer, New York, NY, USA, 2008.
- [14] M. W. Spong and R. Ortega, "On adaptive inverse dynamics control of rigid robots," *IEEE Transactions on Automatic Control*, vol. 35, no. 1, pp. 92–95, 1990.
- [15] P. Chen and Q. Cao, "Trajectory control of the articulated robot based on inverse dynamics," *Journal of Huazhong University of Science and Technology (Natural Science Edition)*, vol. 41, supplement I, pp. 17–20, 2013.
- [16] P. I. Corke, "A robotics toolbox for MATLAB," *IEEE Robotics and Automation Magazine*, vol. 3, no. 1, pp. 24–32, 1996.

- [17] D. Fonte, F. Valente, A. Vale, and I. Ribeiro, "A motion planning methodology for rhombic-like vehicles for ITER Remote Handling operations," in *Proceedings of the 7th IFAC Symposium on Intelligent Autonomous Vehicles (IAV '10)*, pp. 443–448, September 2010.
- [18] A. Vale, D. Fonte, F. Valente, J. Ferreira, I. Ribeiro, and C. Gonzalez, "Flexible path optimization for the cask and plug remote handling system in ITER," *Fusion Engineering and Design*, vol. 88, no. 9-10, pp. 1900–1903, 2013.
- [19] R. Ventura, J. Ferreira, I. Filip, and A. Vale, "Logistics management for storing multiple cask plug and remote handling systems in ITER," *Fusion Engineering and Design*, vol. 88, no. 9-10, pp. 2062–2066, 2013.
- [20] D. Locke, C. Gonzalez Gutierrez, C. Damiani, J.-P. Friconneau, and J.-P. Martins, "Progress in the conceptual design of the ITER cask and plug remote handling system," *Fusion Engineering and Design*, 2014.
- [21] I. A. Şucan, M. Moll, and L. Kavraki, "The open motion planning library," *IEEE Robotics and Automation Magazine*, vol. 19, no. 4, pp. 72–82, 2012.
- [22] J. J. Kuffner Jr. and S. M. la Valle, "RRT-connect: an efficient approach to single-query path planning," in *Proceedings of the IEEE International Conference on Robotics and Automation*, pp. 995–1001, April 2000.
- [23] X. B. Peng, Y. T. Song, C. C. Li, M. Z. Lei, and G. Li, "Conceptual design of EAST flexible in-vessel inspection system," *Fusion Engineering and Design*, vol. 85, no. 7–9, pp. 1362–1365, 2010.
- [24] E. S. Conkur and R. Buckingham, "Clarifying the definition of redundancy as used in robotics," *Robotica*, vol. 15, no. 5, pp. 583–586, 1997.
- [25] N. Ando, T. Suehiro, K. Kitagaki, T. Kotoku, and W. Yoon, "RT-Middleware: distributed component middleware for RT (Robot Technology)," in *Proceedings of the IEEE IRS/RSJ International Conference on Intelligent Robots and Systems (IROS '05)*, pp. 3555–3560, August 2005.
- [26] ITER, *ITER—The Way to New Energy*, 2013, <https://www.iter.org/>.



Hindawi

Submit your manuscripts at
<http://www.hindawi.com>

